JOURNAL OF PROPULSION AND POWER
Vol. 17, No. 4, July–August 2001

Analysis of In-Flight Behavior of Truncated Plug Nozzles

F. Nasuti* and M. Onofri†
University of Rome "La Sapienza," 00184 Rome, Italy

Plug nozzles are usually designed to achieve altitude adaptation in a wide range of chamber/ambient pressure ratios. In actual in-flight operations of plug nozzles, this phenomenon must take place in a flowing airstream, which can affect the performance. To understand the flow behavior in such conditions and to evaluate the departure from the ideal nozzle performance, an investigation is carried out with a validated numerical tool based on the solution of turbulent Navier–Stokes equations and on shock fitting. A sample rocket plug nozzle is analyzed parametrically to evaluate the effect of varying Mach number at constant pressure and the effect of varying pressure ratio at constant Mach number. The results indicate that the interaction with a flowing airstream reduces the pressure of the external air, as seen from the nozzle exhaust jet, yielding a reduction of the performance. In particular, a dramatic decrease of nozzle performance may take place in the transonic region if the slipstream effect is neglected in the design. The results also provide useful indications on how the Mach number and the shroud shape can affect the value of ambient pressure where the transition from open to closed wake takes place.

Nomenclature

A	=	area
C_F	=	thrust coefficient, F/p_cA_t
F	=	thrust
M	=	Mach number
PR	=	pressure ratio, p_c/p_∞
p	=	pressure
r	=	distance from the symmetry axis
T	=	temperature
x	=	distance along the symmetry axis
γ	=	ratio of specific heats
ζ	=	expansion level, expressed as percentage, $\zeta_{\rm do} = {\rm PR}/{\rm PR}_{\rm do}$, $\zeta_{d1} = {\rm PR}/{\rm PR}_{d1}$
η	=	nozzle efficiency, $F/F_{\max}$

Subscripts

a	=	ambient
b	=	base
c	=	chamber
do	=	design value for the overall nozzle
$d1$	=	design value for the primary nozzle
$e1$	=	primary nozzle exit section
max	=	ideal nozzle adapted to ambient conditions
p	=	plug
pb	=	plug base
s	=	shroud
sb	=	shroud base
t	=	throat
tr	=	transition between open and closed wake flow structures
vac	=	vacuum
1	=	primary nozzle
∞	=	ambient freestream values

Introduction

LAUNCHER rocket engines operate in varying ambient conditions and, therefore, need expansion systems capable of yielding high performance in a wide range of chamber-to-ambient pressure ratio values. This requirement has led to many different nozzle concepts, ranging from variable geometries to peculiar external expansion devices. Of course, each proposed concept has its advantages and disadvantages and a tradeoff among technical feasibility, weight, efficiency, and reliability is needed.

In recent times, external expansion nozzles have attracted renewed attention because of the search for highly efficient rocket engines capable of carrying a payload to low Earth orbit by single-stage reusable launchers. One such example is the Lockheed Martin's Venture-Star, in which one of the main technological innovations is the engine, which features a linear truncated plug nozzle to replace the conventional expansion system. The system analyses performed have shown that the advantages of plug nozzles with reference to altitude adaptation can be interesting if a strong saving in weight is obtained by a suitable truncation of the plug, provided this configuration yields only a small reduction of performance compared to the full-length case.

Indeed, if the performance is only slightly decreased by an early truncation of the spike, truncated plug nozzles would permit the design of compact and low-weight motors having very high design expansion ratios. Besides, their altitude adaptation would permit highly overexpanded operations at sea level, avoiding the unreliable behavior that limits the maximum design expansion ratio of conventional nozzles. These two issues make the plug nozzle an ideal candidate for single stage to orbit (SSTO) engines. Indeed, the former issue seems to match the requirements of upper-stage engines, the latter those of a first stage. However, this nozzle is interesting also for multistage rockets.

The goal of the present paper is to investigate the slipstream effects. Indeed, plug nozzles achieve altitude adaptation by the interaction between exhaust gas and external air flowing about the nozzle, while flying at varying Mach numbers. Thus, because the flight speed and the external shape of the nozzle can significantly affect the jet interaction properties, they can affect the nozzle performance as well.[1–6] This is an important aspect to be investigated because the design and first evaluation of performance is often carried out by considering the nozzle operation in still air. Moreover, simple engineering models for predicting the nozzle behavior in the overexpanded range can be created with the assumption of still air,[7] but they may exhibit poor prediction capability because of a strong slipstream effect.

In the present study, an annular rocket plug nozzle configuration is analyzed to evaluate the influence of the flight Mach number and ambient pressure on the main flowfield features and on the nozzle performance, when the freestream ambient pressure yields an overexpanded flow behavior. This operation is the most interesting

Presented as Paper 2000-3289 at the AIAA/ASME/SAE/ASEE 36th Joint Propulsion Conference and Exhibit, Huntsville, AL, 16–19 July 2000; received 10 September 2000; revision received 22 February 2001; accepted for publication 27 February 2001.

*Assistant Professor, Department of Mechanics and Aeronautics, Via Eudossiana 18. Member AIAA.

†Professor, Department of Mechanics and Aeronautics, Via Eudossiana 18. Senior Member AIAA.

case to be studied because in underexpanded conditions the flow behavior and the wall pressure about the plug are independent of the ambient pressure. A parametric analysis is presented, considering numerical solutions at different flight conditions, with a fixed nozzle geometry. Moreover, numerical tests have been carried out to examine the influence of the resolution and turbulence modeling on the solution.

Test Case Description

A single annular plug nozzle geometry is considered for all of the computations performed (Fig. 1). The nozzle is designed to operate with cold gas (air) and with low chamber pressure and temperatures, suited to wind-tunnel testing: $p_c = 790$ kPa and $T_c = 253$ K, respectively.[8] It includes two parts: a primary nozzle, providing the internal expansion for a pressure ratio of $PR_{d1} = 15$, and the plug, which is the central body providing the external expansion.

The primary nozzle geometry is designed to provide parallel flow at its exit in case of inviscid flow, with a flat sonic surface at its throat, that is, the sonic surface is assumed to lie on a plane. This internal expansion is generated by the inner wall curvature, whereas the outer wall geometry is designed as a nonreflecting profile. Similarly, in the external part of the nozzle, the expansion takes place from the primary nozzle lip and propagates toward the plug, whose surface is designed to cancel out these expansion waves. The final theoretical result is a uniform axial flow at the plug exit for design conditions at pressure ratio $PR_{do} = 261$ and still air outside. As mentioned, the theoretical full-length plug would be very long, with the final part being very thin and providing little contribution to thrust. Therefore, the plug has been cut to 20% of its length, yielding the final shape shown in Fig. 1.

In contrast with the still-air behavior assumed as the design condition, the actual in-flight behavior of truncated plug nozzles is more complicated and affected also by the recirculating regions that take place behind the shroud and plug bases. A schematic view of the typical flow features is shown in Fig. 1, where the main flow regions are emphasized by three different gray levels: the white area is the region filled by the exhaust gas, the light gray area is that filled by the external air, and the dark gray areas indicate the separated flow regions behind the plug and shroud bases.

In particular, note that a separated flow at the shroud base region is established that is characterized by low pressure, lower than both the exhaust gas pressure at the primary nozzle exit and the ambient pressure. As a consequence, both the exhaust jet and the external air expand up to the shroud base pressure, whose value depends on the exchange of momentum through the mixing layers. After the expansion, the two jets are directed toward each other and, therefore, they interact, yielding, for instance, in the case of two supersonic jets, the two realignment shocks shown in Fig. 1 (dashed lines). The final direction of the two jets depends on the overall nozzle pressure ratio. It would be a horizontal line in design conditions, whereas the negative slope of the streamlines shown in Fig. 1 indicates overexpanded operations. Of course, the separation line between the two jets (indicated as dividing streamline in the Fig. 1), in reality, is a mixing layer of growing thickness.

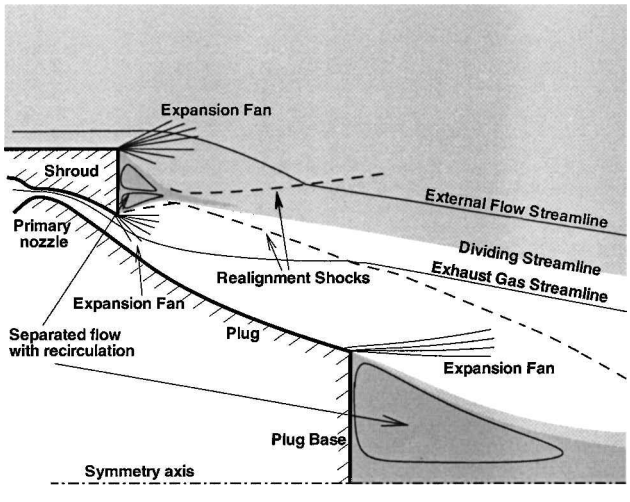

Fig. 1 Main features of truncated plug nozzle flowfield operating overexpanded at supersonic flight speed ($\zeta_{do} = 23.6\%$ and $M_\infty = 2$).

Numerical Approach

Integration Technique

The numerical simulations have been performed by a Navier–Stokes solver developed by the authors. The solver's main feature is to handle shock discontinuities by a fitting technique.[9] In particular, the shock points are explicitly fitted and tracked by a procedure that is an extension of the methodology proposed by Moretti[10] for inviscid flows. It provides a precise prediction of the location and propagation velocity of discontinuities and does not require the introduction of artificial viscosity to achieve stable solutions. That represents an important issue when flowfields with vortices have to be computed. Moreover, in the case of inviscid simulations and viscous simulations in still air, to make the solutions more efficient and accurate, the model replaces the shear layer between exhaust gas and external air by a slip line also treated by a fitting technique.[11]

The methodology is based on the nonconservative form of the Navier–Stokes equations, which are integrated by a second-order time and space accurate scheme that follows Moretti's lambda formulation for the convective terms[12] and that uses central differencing for the viscous terms.[13] A further extension has been recently achieved[14] by implementing the one-equation model of Spalart and Allmaras[15] for turbulent flow simulations.

All computations have been carried out considering the assigned values of p_c and T_c, and, because both the exhaust and ambient gas are air, assuming perfect gas with $\gamma = 1.4$ and viscosity following Sutherland's law. An adiabatic wall has been assumed for all viscous simulations. A typical grid used for computations is shown in Fig. 2, where the cell distribution and the partition of the flowfield in suitable blocks can be observed, all featuring orthogonal meshes.

The flow structures discussed in the preceding section are characterized by large recirculating regions bounded by mixing layers. These structures represent one of the more challenging problems to be solved by computational fluid dynamics because of the role of turbulence in establishing the average pressure in a base region, because of the slow convergence rate, and because of the necessity of a huge number of cells to reach grid-independent solutions. Therefore, a thorough evaluation of the turbulence model performance and of the grid resolution needed is required to substantiate the results, as reported hereafter.

Turbulence Model

The comparison between the base pressure predicted by using the model of Spalart and Allmaras[15] and experimental data is discussed in Ref. 14, where the improvement of the results obtained by a simple compressibility correction necessary to provide a suitable simulation of compressible mixing layers is also shown. Further developments have led to a more general model for compressibility correction based on the convective Mach number.[16,17]

To provide an idea of the role played by the compressibility correction in plug nozzle flows, the comparison of results obtained with

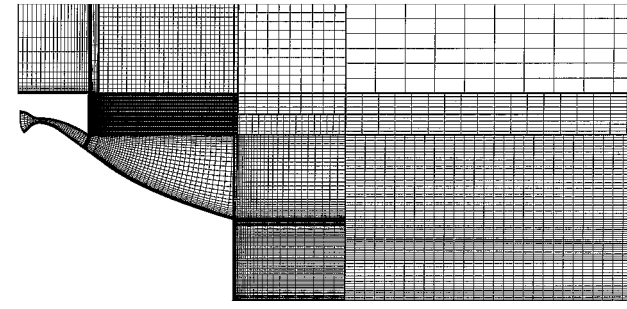

Fig. 2 Computational grid.

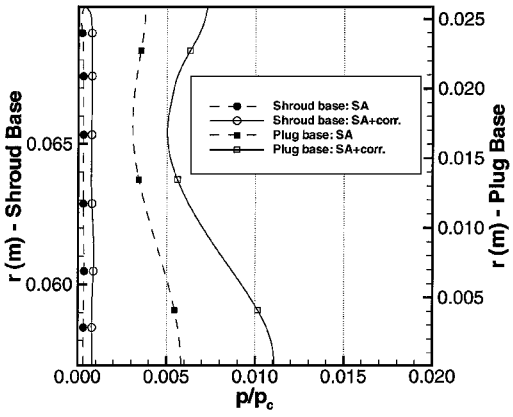

Fig. 3 Computed wall pressure on shroud base (left axis) and on plug base (right axis).

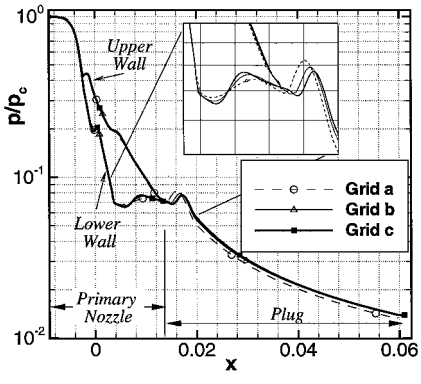

Fig. 4 Computed wall pressure on primary nozzle and plug walls.

and without correction are shown in Fig. 3, for the case of $M_\infty = 2$, PR = 61.7, and $T_\infty = 164$ K. The computed wall pressure on the shroud base shows in both cases low values with a flat behavior. Nevertheless, it is worth stressing that the average value obtained with the compressibility correction is about 2.5 times greater than that obtained with the model of Spalart and Allmaras without any correction. A similar behavior is obtained at the plug base, where there is a factor of about two between the average base values. Although in the latter comparison the effect of the flow in the shroud base region on the plug base pressure values should also be considered, the comparison indicates that the compressibility effect cannot be neglected in plug nozzle flow computations.

Resolution

For the analysis of the present plug nozzle flowfields, it is also important to verify the grid independence of the solution, which could be questionable because of the presence of large recirculating regions. In this framework, a set of computations, including the compressibility correction in the turbulence model, has been carried out for three different grid levels, with the two finer levels obtained from the coarser level (shown in Fig. 2), by increasing the number of cells in each direction by a factor of 1.5 and 2, respectively (Table 1). The present analysis has been carried out for the following flow conditions: $M_\infty = 2$, PR = 61.7, and $T_\infty = 164$ K.

The results show that the first grid level is too coarse because there are significant displacements in comparison to the solution provided by the finer grids. Conversely, the second level shows results satisfactorily close to the next level, and, thus, it has been chosen as the reference. These conclusions are substantiated by Figs. 4 and 5. Figure 4 shows the pressure behavior on the primary nozzle walls and on the plug wall up to the truncation point. Note that there are only minor differences among the solutions, emphasized by the enlargement of the plateau region in the lower wall that takes place between the internal and external expansion regions.

Similar results have been obtained for base pressures. Figure 5 shows that there is a displacement in the shroud base pressure prediction between the two coarser grids, whereas grid b and grid c show nearly identical pressure behaviors. Indeed, the average shroud base pressure value passes from 640 Pa (grid a) to 713 Pa (grid b, grid c), with differences less than 1 Pa between grid b and grid c. Also, the plug base pressure does show that the resolution of grid b is sufficient to provide results close to the grid-independent limit. In particular, the main result of increasing resolution is a flatter profile while yielding only slight changes in the average pressure value that passes from 5123 Pa (grid a) to 5206 Pa (grid b, 1.5% difference).

Table 1 Computational grids considered and number of cells

Grid	Cell ratio	Number of cells		
		Plug	Wake	Total
a	1.0	21,784	7,044	28,828
b	1.5	49,014	15,714	64,728
c	2.0	87,136	0	87,136

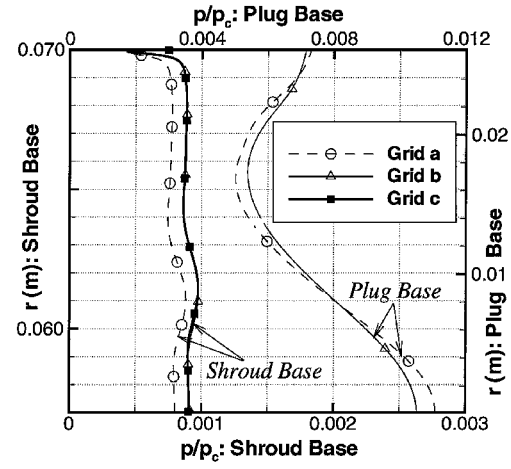

Fig. 5 Computed wall pressure on shroud base (left axis) and on plug base (right axis).

Basic Effects of Freestream

The major effect of the freestream on plug nozzles is a reduction of performance in the overexpanded range, with possible abrupt changes in the transonic regime. This can be illustrated by the inviscid analysis of a simplified nozzle geometry. In particular, it has been assumed that the external shape of the nozzle wall ends with a wedge, thus, the effect of the generation of a base flow region behind the shroud has been neglected. Moreover, because the preliminary analysis is focused on the interaction between the exhaust gas and the external air, the plug nozzle base region has also been neglected. This way, a numerical solution obtained by a coarse mesh, containing only 1856 cells, is sufficient to detect and emphasize the differences in nozzle performance due to the external stream.

The analysis is performed assuming the freestream ambient pressure as constant and for varying freestream Mach number. In particular, a highly overexpanded operating condition has been considered with PR = 16.7 ($\zeta_{do} = 6.4\%$), to yield a slight underexpanded behavior ($\zeta_{d1} = 110.5\%$) of the primary nozzle. In this case only a small part of the plug profile is reached by the expansion waves generated at the primary nozzle lip, even for the short plug considered, truncated at 20% of the ideal length. Therefore, any change in the external flow yields a clear effect on the plug, rendering the analysis easier.

The computed Mach number contour lines and the relevant streamlines are displayed in Fig. 6 for four different values of the external stream Mach number, ranging from still to subsonic and eventually to supersonic values. A different flow behavior takes place depending on the subsonic or supersonic value of the freestream Mach number, and, therefore, the relevant flowfields are discussed separately hereafter.

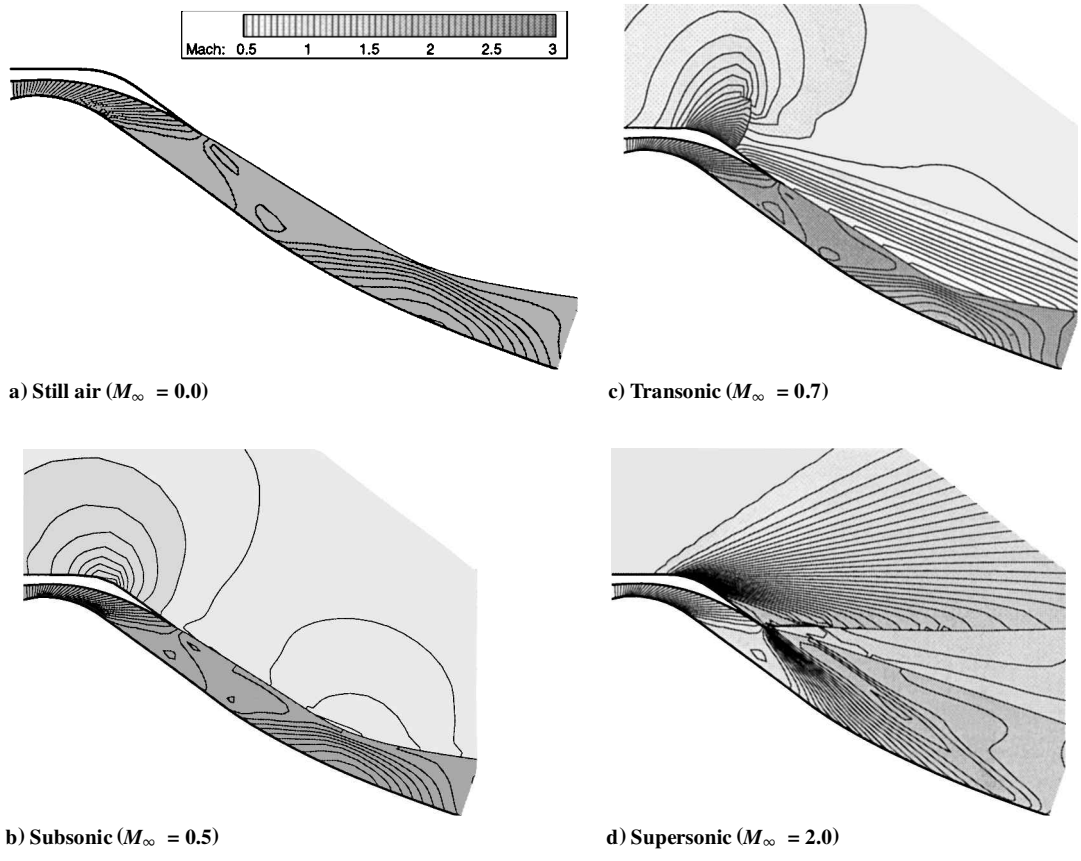

Fig. 6 Comparison of inviscid simulations at PR = 16.7 and different M_∞ : Mach number contour lines.

Subsonic Freestream

In the still-air case, a weak expansion occurs at the lip that propagates toward the plug (Fig. 6a) without generating any reflection because of the suitable concave profile. Downstream the end of this expansion the same concave plug wall acts like a supersonic ramp, generating compression waves that interact with the jet boundary, causing it to bend upward with a consequent generation of reflected expansion waves. The analysis of wall pressure shows this behavior clearly (Fig. 7a). In particular, it shows a minimum at $x = 0.006$ m, then a peak at $x = 0.026$ m, and finally the wall pressure decreases again because of the reflected expansion waves. Note that the plug wall pressures computed for all of the subsonic cases show only slight deviations from the still air case (Fig. 7a). The slight differences among the curves indicate that the external air does not behave as a constant pressure environment: The analysis of the flowfield displayed in Fig. 6b indicates that the external stream expands around the convex corner of the shroud, but before its end it recompresses because of the interaction with the nozzle exhaust jet. Figure 7b shows that at the shroud lip ($x = 0$ m) the pressure value is nearly equal to the still-air case, although a closer analysis evidences that there is a little overexpansion. Downstream, as can be seen in Fig. 6b, the interaction between the compression waves coming from the plug surface and the external subsonic flow yields a weak compression region, also on the external side, explaining the slight discrepancies among the pressure plots of the subsonic cases in Fig. 7a.

The plug-wall pressure in the transonic region ($0.7 < M_\infty < 1.0$) does not show significant differences in comparison with the still-subsonic behavior (Fig. 7a). Nevertheless, a different flow structure can be noticed on the shroud wall. Indeed, the external flow expanding about the shroud becomes supersonic, and then it recovers its freestream pressure by a curved shock wave (Fig. 6c). Therefore, as shown in Fig. 7b, the shroud-wall pressure decreases to values significantly lower than freestream, and then suddenly, as a result of a shock, it jumps to values close to p_∞.

Supersonic Freestream

At supersonic values of M_∞ the plug- and shroud-wall pressures show a behavior significantly different than in the subsonic range. The external flow expands about the shroud as shown in Fig. 7b by the two lower curves, marked by squares, relevant to the supersonic tests: the higher M_∞, the greater the expansion.

Downstream, at the primary nozzle lip, the two supersonic flows, the external air and the exhaust jet, interact. As in the case considered, $p_\infty < p_{e1}$, at the primary nozzle lip the external air shows a pressure $p_a < p_\infty < p_{e1}$ because of the expansion about the shroud. Therefore, the interaction of the two supersonic jets generates a compression of the external flow (oblique shock in Fig. 6d) and an expansion of the primary nozzle exhaust jet, such that the flow exhibits a pressure value $p_a < p < p_{e1}$ downstream of the interaction. The analysis of the plug-wall pressure behavior (Fig. 7a) shows that in the supersonic case the exhaust jet experiences a stronger expansion than in the subsonic air cases. This means that after recompression through the oblique shock wave, the ambient pressure resulting from the external/internal jet interaction is still lower than p_∞.

As main consequence of the pressure behavior at lip, the plug-wall pressure can become lower than p_∞, yielding a negative contribution to thrust. In particular, for increasing Mach numbers the expansion experienced by the exhaust jet increases. Figure 7a shows that at $M_\infty = 1.3$ a limited part of the plug wall is covered by the expansion fan, whereas at $M_\infty = 2$ the expansion waves generated at the primary nozzle lip impinge on almost the whole plug wall. This allows us to conclude that, in the supersonic range, the higher M_∞, the larger the plug-wall zone with $p < p_\infty$, the lower the average plug-wall pressure, and, thus, the higher the negative contribution of plug to thrust.

Nozzle Performance

The analysis of the computed nozzle performance reported in Table 2 shows a strong slipstream effect. In particular, in Table 2,

Table 2 Computed slipstream effect on performance

M_∞	$C_{F,1}$	$C_{F,p}$	$C_{F,s}$	C_F	C_F^a	η	η^a
0.0	1.10	0.20	0.00	1.30	1.30	0.98	0.98
0.5	1.10	0.21	−0.04	1.31	1.27	0.99	0.96
0.7	1.10	0.20	−0.08	1.30	1.22	0.98	0.92
0.9	1.10	0.20	−0.16	1.30	1.14	0.98	0.86
1.3	1.10	−0.13	−0.19	0.97	0.78	0.74	0.59
2.0	1.10	−0.14	−0.21	0.96	0.75	0.72	0.57

[a]Includes shroud drag.

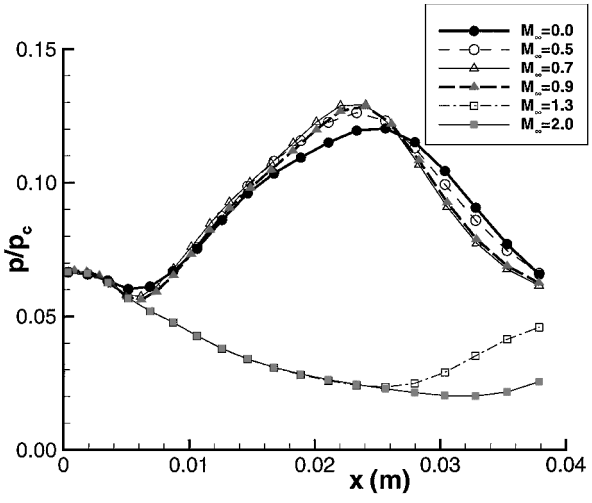

a) Plug

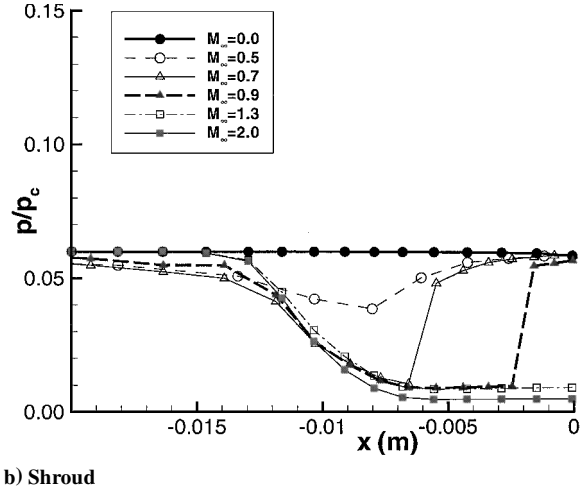

b) Shroud

Fig. 7 Computed wall pressure.

the primary nozzle contribution to thrust, the plug contribution, the shroud drag, the total thrust without accounting for the shroud drag, and the total thrust including the shroud drag are listed as a function of Mach number. The total efficiencies with and without the shroud contribution are also reported.

One of the most interesting indications from Table 2 is the low efficiency in the supersonic range, even if shroud drag is neglected. Indeed, as discussed, the ambient pressure faced by the exhaust jet after interaction with the supersonic external stream is lower than p_∞ and decreases with increasing M_∞. On the other hand, in the subsonic tests the resulting pressure at the external/internal jet interaction shows values close to p_∞. Thus, the plug contribution does not change significantly, and the slipstream effect is only an increase of the shroud drag for increasing M_∞.

Note that the changes within both the subsonic and supersonic regimes are small in comparison with the big jump occurring when the external flow passes from subsonic to supersonic. Also note that the aforementioned differences take place at highly overexpanded conditions, whereas they would shrink, up to vanishing point, for increasing PR, except for the shroud drag contribution. This means that an abrupt change of performance of the plug nozzle is actually expected if it reaches the transonic region in the overexpanded regime ($PR_{d1} < PR < PR_{do}$) and also that this change is expected to be greater the lower the PR in the transonic regime because of the larger extension of the plug region involved.

Flow Features and Wake Structure in Still Air

To analyze the consequence of having flowing airstream instead of still air, it is useful to recall the main flow structures that occur in the latter case.[18,19] Figure 8 shows the computed solutions in still air for four different pressure ratios. The mixing layer between the exhaust gas and the ambiance is replaced by a slip line, behaving like a constant pressure boundary, computed by a fitting technique.[11] The computation has been carried out by the Navier–Stokes solver, with the turbulence model without the compressibility correction; therefore, the calculated base pressure is lower than the expected actual value. However, these assumptions do not change the main qualitative aspects of the flowfield considered in the present discussion.

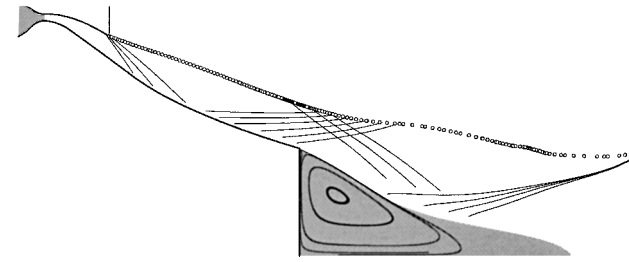

a) PR = 39.5 (ζ_{do} = 15.1%)

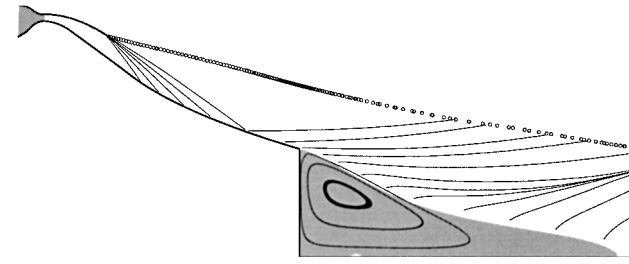

b) PR = 61.7 (ζ_{do} = 23.6%)

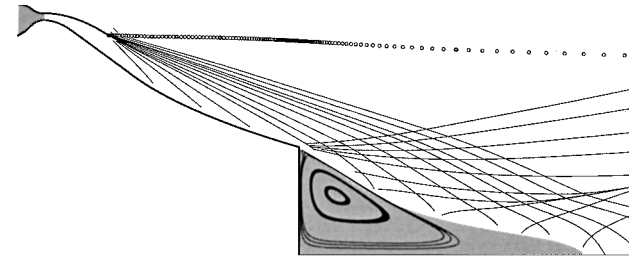

c) PR = 202.6 (ζ_{do} = 77.6%)

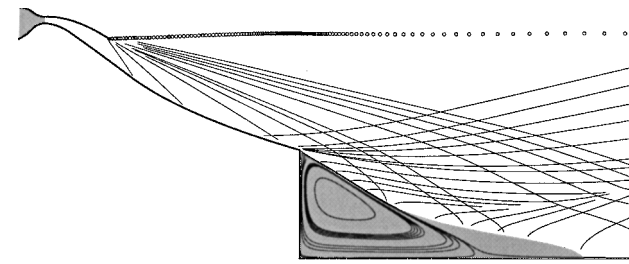

d) PR = 292.6 (ζ_{do} = 112.1%)

Fig. 8 Truncated plug nozzle flowfield in still air: subsonic regions (filled areas), characteristic waves, and closed streamlines.

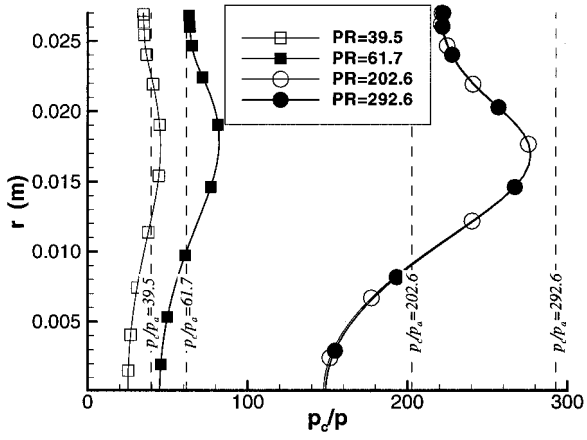

Fig. 9 Computed base pressure in still air for varying PR, dashed lines indicate ambient pressure value (p_a) for each PR considered.

Figure 8a shows a highly overexpanded case. It can be seen that although the value of PR greater than in Fig. 6 allows a wider expansion at the primary nozzle lip, the last characteristic wave emanating from that lip still impinges on the plug wall. As a consequence, the latter part of the wall behaves like a supersonic ramp yielding compression waves. These waves impinge on the jet constant-pressure boundary and, thus, they reflect as expansion waves, impinging in turns on the wake generated behind the plug base. It is evident that any change in ambient pressure yields a consequent change of flow properties in the plug base region, where, therefore, base pressure depends on ambient pressure. This is a clear example of the flow structure known as open wake, defined such that for varying PR the average base pressure changes with the ambient pressure, although a closed bubble takes place behind the base.[7] The average base pressure shows values close to the ambient value (Fig. 9).

The second case, shown in Fig. 8b, is less overexpanded. The expansion at the primary nozzle lip cover almost the whole plug wall, such that it no longer generates compression waves, as indicated by the characteristic waves and by the straight jet boundary. It is again an example of open wake, whose recirculating region at the plug base is bounded by a supersonic jet with $p \simeq p_a$.

The following two plots (Fig. 8c and Fig. 8d) show the flow structure known as closed wake, occurring at the higher PR range, although starting from values lower than design. Indeed, it can be seen that in these cases the last expansion wave emanating from the primary nozzle lip impinges on the wake downstream of the sonic line and, therefore, any change in ambient pressure between the two PR and toward higher PR does not affect the subsonic region behind the plug base. The consequence is that the base pressure is independent of the ambient pressure for PR $\geq$ 202.6, as clearly shown in Fig. 9. Note that the value of PR = 202.6 considered in Fig. 8c should be close to the value of PR where the flow structure changes between closed and open wake (PR_{tr}). This is indicated by Fig. 9 where, for PR = 202.6, the plug base pressure coincides with that obtained at higher PR (closed wake behavior) and has an average value close to ambient pressure (open wake behavior).

Flow Features and Wake Structure in Supersonic Stream

During actual flight conditions the behavior of the engine shows significant differences in comparison with the still air case, as shown by Figs. 1 and 8. The main difference with the still-air case is the generation of a separated flow at the shroud base region, which is characterized by low pressure and two counter-rotating vortices. As in the case of inviscid flow over a zero-thickness shroud, the presence of a supersonic stream yields a low-pressure region about the shroud and then a reduction of the ambient pressure seen by the jet exhausting from the primary nozzle. This is shown by comparing the flowfield computed for a supersonic airstream ($M_\infty = 2$, upper side of Figs. 10 and 11) and still air (lower side) at the same ambient and chamber conditions, with PR = 61.7 ($\zeta_{do} = 23.6\%$) and $T_\infty = 164$ K.

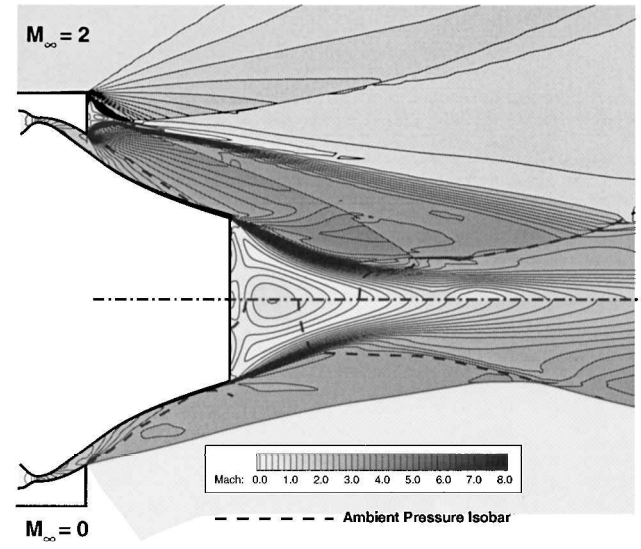

Fig. 10 Comparison of plug nozzle flowfields in still air (down) and supersonic airstream (up); Mach number contour lines and ambient pressure isobar; PR = 61.7 and T_∞ = 164 K.

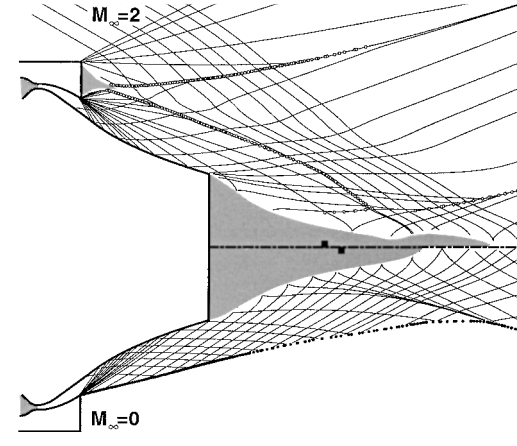

Fig. 11 Computed characteristic lines, shocks (○), subsonic regions (gray areas), and stagnation points (■) for a plug nozzle in a supersonic stream (up) and in still air (down, ● = jet boundary); PR = 61.7 and T_∞ = 164 K.

The ambient pressure isobars displayed over the flowfield by a thick dashed line in Fig. 10 can be helpful in emphasizing the slipstream effect. The still-air solution shows that the base pressure is nearly equal to the ambient pressure. In particular, the ambient pressure isobar impinges on the plug wall and, downstream, the remaining part of the plug acts as a slightly compressing surface. However, only a small part of the plug wall is free from the expansion waves coming from the primary nozzle lip, and, thus, it yields such a weak compression that it cannot be detected by the characteristic net of Fig. 11. Note that downstream of the ambient pressure isobar the flowfield shows nearly constant pressure (notice also the parallel characteristic waves in Fig. 11) that acts also on the base flow region. Only at the wake neck must the flow compress and the pressure becomes higher than ambient through the trailing shock. On the contrary, in the $M_\infty = 2$ case, the driving mechanism of the expansion is the shroud base pressure value, which is lower than the ambient pressure. Therefore, the expansion covering the plug wall continues downstream of the ambient pressure isobar, so that a part of the plug and the base region are affected by pressure lower than ambient.

Therefore, at the same nozzle pressure ratio, the solution with $M_\infty = 2$ represents a typical case of closed wake flow structure, with a base pressure value independent of p_∞ for increasing PR, whereas an open wake takes place with $p_{pb} \simeq p_\infty$ in the case of still

air. In this case, because the closed wake value of p_{pb} is much lower than p_∞, the base drag in supersonic flight conditions is higher than the one predicted at rest.

The different wake structure at the same PR indicates that a different mechanism drives the transition from open to closed wake in the presence of an external stream. In fact, in the still-air case, it has been shown in Ref. 7 that the transition takes place when the last characteristic wave emanating from the primary nozzle lip impinges on the nozzle axis ahead of the stagnation point region. Conversely, in the in-flight case, the same role is played by the lower realignment shock, emanating from the shroud base region, often referred to as envelope[6] or internal[20] shock. Indeed, it represents the boundary of the expansion process emanating from the shroud base, and, thus, it is the signal closest to the plug among those carrying information about the ambient pressure value. This can be seen in the upper side of Fig. 11, where the characteristic waves also show that the expansion at the plug base lip bends the internal shock toward the axis. Note that the expansion waves emanating from the primary nozzle lip would not reach the subsonic region behind the base, whereas the internal shock impinges on the subsonic wake region making it extend further downstream.

However, in the particular case shown in the upper side of Fig. 11, the wake structure can still be considered closed because the wake region upstream of the stagnation point (filled square in Fig. 11) is not affected by any information about the ambient pressure, as conversely happens when the shock impinges on the wake in a point closer to the plug base than the stagnation point neighborhood.[7] The latter case is shown, for instance, in the lower side of Fig. 11, where all of the characteristic waves impinging on the subsonic base region carry information about the ambient pressure value from the jet boundary.

In conclusion, in the case of an external stream, the indicator of the influence of the external ambient is the internal shock rather than the last characteristic line of the lip expansion fan. Therefore, the engineering model introduced in Ref. 7 to predict the value PR_{tr} of the nozzle pressure ratio at which the transition from open to closed wake takes place should be adequately extended to the case of in-flight operations, to compute more properly the impingement point of the first signal carrying the ambient pressure information.

Evaluation of Flow Evolution Along the Flight Path

Further interesting effects of the external flow can be seen by the analysis of the flowfield at varying freestream Mach number, passing from zero to subsonic values, then to supersonic, and finally to different values in the supersonic regime. The analysis is carried out by reducing the Mach number in the supersonic range from the highest value considered while keeping constant the exhaust gas properties and the ambient pressure.

The main effect of reducing M_∞ is the increase of the shroud base pressure because of the enlargement of the dead-air region with the two counter-rotating vortices and of a lower expansion of both the exhaust jet and the external stream (Fig. 12). In particular, weaker expansions of both jets at the primary nozzle and shroud lips result in smaller flow rotations (smaller lip rotation angle in Fig. 12) and also in lower Mach numbers of the two jets at the stagnation point. These lower Mach numbers upstream of the stagnation point yield larger angles between the realignment shocks and the dividing streamline.

Actually, note that the final direction of these shocks is affected also by the smaller realignment angles to turn the jets back downstream of the stagnation point. Indeed, because the average jet direction downstream of the interaction with the external stream (the dividing streamline in Fig. 12) mainly depends on the overall pressure ratio and is nearly independent of the external Mach number (i.e., also of the shroud base pressure), smaller lip rotation angles require smaller realignment angles. Nevertheless, it can be seen that the variation of the realignment angles has only a slight effect on shock angles, whose variation is mainly due to the changes of Mach numbers at the stagnation point, upstream of the interaction.

The computed profiles of realignment shocks are shown for three different supersonic Mach numbers, along with the extension of the dead-air region and the final jet direction, in Fig. 13. The result

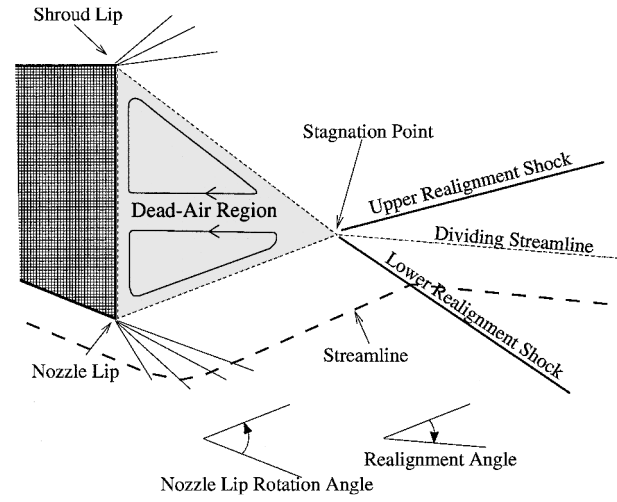

Fig. 12 Schematic view of main flow features about shroud base.

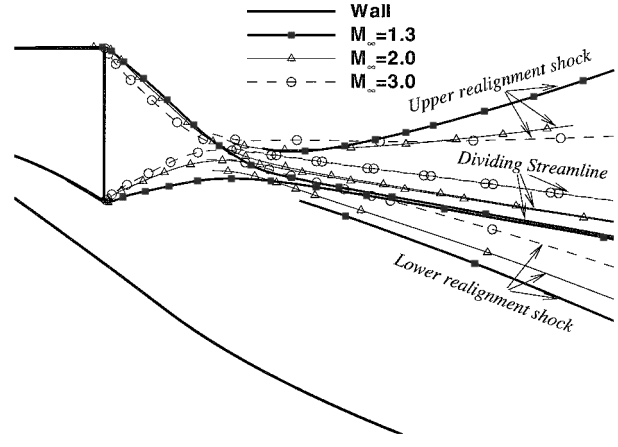

Fig. 13 Computed streamlines and shocks about shroud base for M_∞ = 1.3, 2.0, and 3.0; PR = 61.7 (ζ_{do} = 23.6%); and T_∞ = 164 K.

confirms that the shocks depart from each other as M_∞ decreases because of the lower expansion about the shroud base for both supersonic streams. The main consequence is that the lower shock angle increases its module and consequently will impinge on the wake at lower abscissas. The computations confirm that the jet direction after interaction is almost insensitive to M_∞, but they also indicate that there is a translation of the dividing streamline toward the plug that yields a further inner displacement of the internal shock for decreasing M_∞. These considerations may become important when trying to develop a model for the prediction of open/closed wake transition because, as mentioned, the shock is the first wave carrying the ambient pressure information to the base region.

The further reduction of Mach number from supersonic to subsonic values yields a major change in the flow structure behind the shroud. In fact, the plug nozzle flowfield in subsonic flight conditions is quite similar to the case of still air. Only a slight overexpansion of the exhaust jet takes place in the case of $M_\infty = 0.7$, shown in Fig. 14, although the external jet becomes locally supersonic because of its expansion at the shroud lip. In the subsonic case the recirculating region at the shroud base is quite large and is dominated by the upper, clockwise-rotating vortex, whereas in the supersonic case the separated region is smaller and is dominated by the two counter-rotating vortices with similar dimensions. Both structures agree with experimental data obtained for similar test cases in Ref. 21 for the subsonic case and in Ref. 22 for the supersonic case, respectively.

Concerning the plug base, note that the increase of shroud base pressure for decreasing Mach number changes the features of the interaction between ambient and plug base region (see Fig. 15 and Table 3). In fact, the wake is clearly closed at $M_\infty = 3$ because the

internal shock impinges on the wake when it has already become supersonic. On the other hand, it cannot be considered closed at $M_\infty = 2$, as shown in Table 3 by the increased average pressure value on the plug base, in comparison to $M_\infty = 3$. Note, however, that despite the open wake structure the average base pressure is considerably lower than ambient pressure. This is because the average pressure in the exhaust jet bounding the wake is lower, due to the overexpansion at the shroud, and the internal shock impinges only on the downstream part of the wake. A further decrease of M_∞, still in the supersonic range, yields a regression of the internal shock with consequent increase of plug base pressure ($M_\infty = 1.3$), although the influence of the shroud still makes p_{pb} lower than p_a.

A different behavior is shown in the subsonic case, where the average base pressure on the shroud is closer to the ambient pressure value. The consequence is that the exhaust jet does not overexpand significantly, as in the case of still air, and, thus, there is a direct influence of ambient pressure on the wake.

To evaluate the influence of the variation of M_∞ on the overall engine performance, a schematic of the general behavior of base contribution to thrust is plotted in Fig. 16. The following discussion is only indicative of the variations of the contribution of plug base to thrust and should be complemented by the contribution of the remaining part of the plug and of the shroud. However, the following simple analysis could be helpful in understanding the expected trends.

The average pressure acting on the plug base does not change in the closed wake regime, where for increasing PR the base contribution to thrust increases only because of the ambient pressure reduction, reaching its maximum in vacuum. The behavior of $C_{F,pb}$ as a function of PR is, therefore, represented by a hyperbola in Fig. 16. To emphasize the reduction of $C_{F,pb}$ in the presence of a freestream of increasing M_∞, it has been assumed that in the open wake regime in still air the average pressure on the plug base is equal to the ambient pressure. Thus, $C_{F,pb} = 0$ for an open wake in still air.

In case of in-flight conditions, the open wake behavior has been depicted in Fig. 16 by an arbitrary curve connecting the lower PR conditions (where it has been assumed for the sake of simplicity that $p_{pb} \simeq p_a$ and $C_{F,pb} = 0$), to the transition point on the closed wake hyperbola (where p_{pb} takes its closed wake value). Figure 16 shows behaviors representative of three different values of M_∞, in

Table 3 Computed value of average pressure on the plug and shroud bases: p_∞ = 12,800 Pa, PR = 61.7 (ζ_{do} = 23.6%), and T_∞ = 164 K

M_∞	p_{sb}, Pa	p_{pb}, Pa	Wake
0.0	12,800	11,568	Open
0.7	9,261	16,160	Open
1.3	1,348	7,074	Open
2.0	713	5,206	Open
3.0	404	4,543	Closed

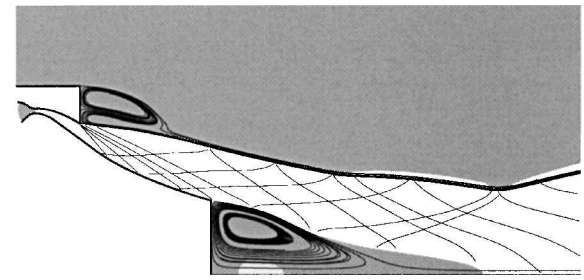

a) M_∞ = 0.7

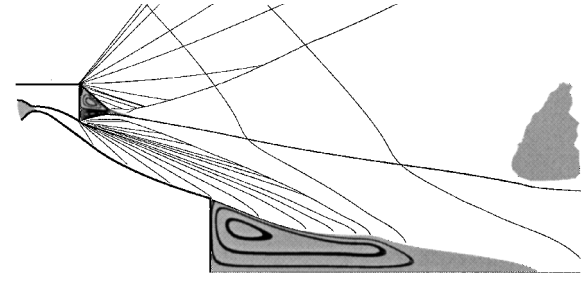

b) M_∞ = 1.3

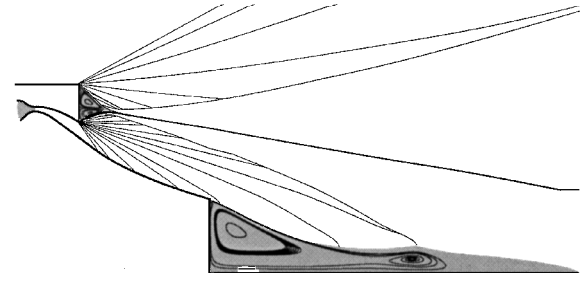

c) M_∞ = 2.0

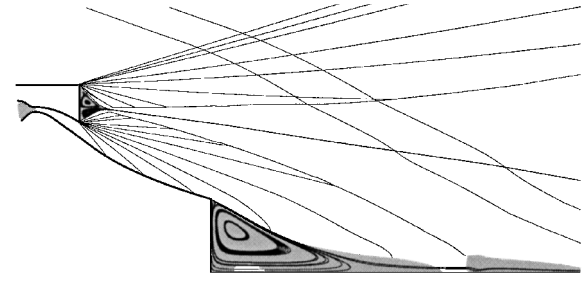

d) M_∞ = 3.0

Fig. 15 Truncated plug nozzle flowfield in flowing airstream: subsonic regions (filled areas), characteristic waves, and closed and dividing streamlines (PR = 61.7, ζ_{do} = 23.6%, and T_∞ = 164 K).

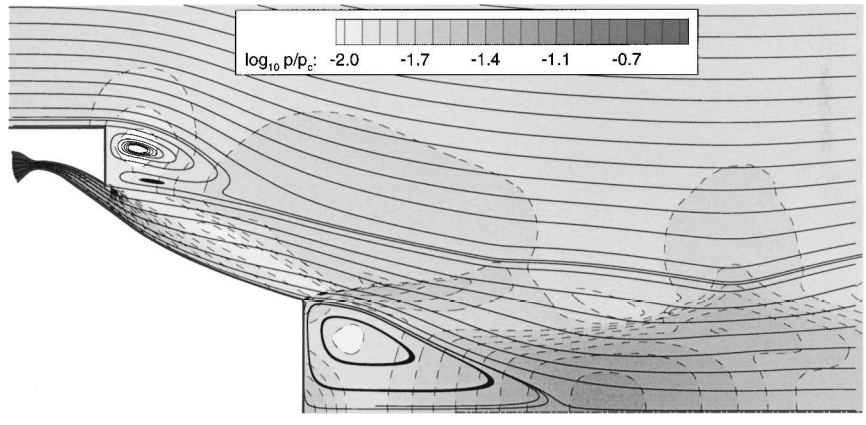

Fig. 14 Main features of a truncated plug nozzle flowfield operating overexpanded at subsonic flight speed (PR = 61.7, ζ_{do} = 23.6%, M_∞ = 0.7, and T_∞ = 164 K).

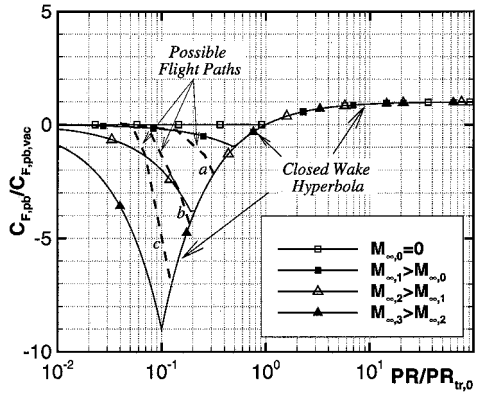

Fig. 16 Schematic of contribution to thrust (or drag) of plug base; numbers and curves are only displayed to show general behavior and do not pretend to represent any real nozzle.

addition to the still-air case. Note that the base drag takes place for a larger range of PR and increases for increasing M_∞.

In the case of a launch vehicle, PR and M_∞ increase along the flight path. Therefore, the evolution of $C_{F,\mathrm{pb}}$ will follow lines connecting points of the curves at $M_\infty = \text{const}$, corresponding to the pairs of values of M_∞ and PR, taken along the trajectory. Such behaviors are shown, for instance, by the dashed lines in Fig. 16, each indicative of a different flight path. In particular, they indicate increasing acceleration moving from *a* to *c* and suggest that the higher the vehicle acceleration, the steeper the dashed line, the higher the base drag that would occur in the first part of the flight.

Conclusions

The numerical analyses performed indicate that the interaction of the exhaust jet with the external air in truncated plug nozzles may significantly affect the nozzle behavior in the overexpanded regime. In particular, it has been shown that, also in the ideal case of a zero-thickness shroud and inviscid flow, important losses take place that can yield a sudden performance drop if the sonic transition is achieved at PR closer to the design value of the primary nozzle than to the design value of the overall nozzle. The presence of a finite thickness or thick shroud substantially changes the flow behavior, adding further drag in itself and yielding an overexpansion at the primary nozzle lip. Because of this overexpansion, the exhaust jet finds at the lip a lower ambient pressure than in the still-air case and consequently adapts the flow to a lower-than-ambient pressure. This is a further cause of drag that appears in part over the plug wall and in part over the plug base. Moreover, the overall nozzle performance is reduced because of the reduction of the value of PR for transition from open to closed wake. This reduction yields a base drag in the range between the actual and still-air transition values. With regard to the mechanism of wake transition, it has been shown that in the supersonic case the transition is governed by the internal shock, rather than by the last wave of the expansion fan at the primary nozzle lip. On the contrary, the analysis of flowfield in the subsonic flight conditions has shown that only slight changes are expected in comparison to the still-air case. Finally, the effects of the freestream M_∞ have been studied, analyzing its impact on the flow structure at the shroud and on the internal shock, as well as on the contribution to plug base drag.

Acknowledgments

The present study has been partially financed by the ESA in the framework of Technology and Research Projects under European Space Research and Technology Centre/Contract n.12514/76/NL/FG, the Italian Space Agency, and the Italian Ministry for Technological and Scientific Research. The authors wish also to acknowledge the contribution of Renato Paciorri to the development of the turbulence model used in the computations.

References

[1]Valerino, A., Zappa, R., and Abdalla, K., "Effects of External Stream on the Performance of Isentropic Plug-Type Nozzles at Mach Numbers of 2.0, 1.8, and 1.5," NASA Memo 2-17-59E, March 1959.

[2]Mercer, C. E., and Salters, L. B., "Performance of a Plug Nozzle Having a Concave Central Base with and Without Terminal Fairings at Transonic Speeds," NASA TN D-1804, May 1963.

[3]Wasko, R., "Performances of Annular Plug and Expansion Deflection Nozzles Including External Flow Effects at Transonic Mach Numbers," NASA TN D-4463, April 1968.

[4]Beheim, M. A., and Boksenbom, A. S., "Variable Geometry Requirements in Inlets and Exhaust Nozzles for High Mach Number Applications," NASA TM X-52447, Sept. 1968.

[5]Mercer, C. E., and Burley, J. R., "Performance Characteristics of an Isolated Coannular Plug Nozzle at Transonic Speeds," NASA TM-87606, Oct. 1985.

[6]Ruf, J. H., and McConnaughey, P., "Plume Physics Behind Aerospike Nozzle Altitude Compensation and Slipstream Effect," AIAA Paper 97-3218, July 1997.

[7]Nasuti, F., and Onofri, M., "Theoretical Analysis and Engineering Modeling of Flowfields in Clustered Module Plug Nozzles," *Journal of Propulsion and Power*, Vol. 15, No. 4, 1999, pp. 544–551; also AIAA Paper 98-3524, July 1998.

[8]Rydén, R., "GSTP Test Case Description," ESA/European Space Research and Technology Center, Sept. 1999, pp. 1–10.

[9]Nasuti, F., and Onofri, M., "Analysis of Unsteady Supersonic Viscous Flows by a Shock Fitting Technique," *AIAA Journal*, Vol. 34, No. 7, 1996, pp. 1428–1434; also AIAA Paper 95-2159, June 1995.

[10]Moretti, G., "Efficient Euler Solver with Many Applications," *AIAA Journal*, Vol. 26, No. 6, 1988, pp. 655–660.

[11]Nasuti, F., Niccoli, R., and Onofri, M., "A Numerical Methodology to Predict Exhaust Plumes of Propulsion Nozzles," *Journal of Fluids Engineering*, Vol. 120, No. 3, 1998, pp. 741–750.

[12]Moretti, G., "A Technique for Integrating Two-Dimensional Euler Equations," *Computer and Fluids*, Vol. 15, No. 1, 1987, pp. 59–75.

[13]Moretti, G., Marconi, F., and Onofri, M., "Shock Boundary Layer Interactions Computed by a Shock Fitting Technique," *Lecture Notes in Physics*, Vol. 414, Springer-Verlag, Berlin, 1993, pp. 345–349.

[14]Nasuti, F., Paciorri, R., and Onofri, M., "Computation of Turbulent Supersonic Base Flows by a Shock-Fitting Quasi-Linear Solver," American Society of Mechanical Engineers, Paper FEDSM99-7316, July 1999.

[15]Spalart, P. R., and Allmaras, S. R., "A One-Equation Turbulence Model for Aerodynamic Flows," *La Recherche Aerospatiale*, No. 1, 1994, pp. 5–21.

[16]Paciorri, R., Nasuti, F., and Sabetta, F., "Evaluation of Turbulence Modeling in Supersonic Afterbody Computations," AIAA Paper 2001-3039, June 2001.

[17]Samimy, M., and Elliott, G. S., "Effects of Compressibility on the Characteristics of Free Shear Layers," *AIAA Journal*, Vol. 28, No. 3, 1990, pp. 439–445.

[18]Nasuti, F., and Onofri, M., "Methodology to Solve Flowfields of Plug Nozzles for Future Launchers," *Journal of Propulsion and Power*, Vol. 14, No. 3, 1998, pp. 318–326; also AIAA Paper 97-2941, July 1997.

[19]Immich, H., Nasuti, F., Onofri, M., and Caporicci, M., "Experimental and Numerical Analysis of Linear Plug Nozzles," AIAA Paper 98-1603, April 1998.

[20]Sule, W., and Mueller, T., "Annular Truncated Plug Nozzle Flowfield and Base Pressure Characteristics," *Journal of Spacecraft*, Vol. 10, No. 11, 1973, pp. 689–695.

[21]Benay, R., and Servel, P., "Applications d'un Code Navier–Stokes au Calcul d'Écoulements d'Arriére-Corps de Missiles ou d'Avions," *La Recherche Aerospatiale*, No. 6, 1995, pp. 405–426.

[22]Amatucci, V. A., Dutton, J. C., Kuntz, D. W., and Addy, A. L., "Two-Stream, Supersonic, Wake Flowfield Behind a Thick Base, Part I: General Features," *AIAA Journal*, Vol. 30, No. 8, 1992, pp. 2039–2046.